Supporting Information for

Non-spherical microparticle shape in Antarctica during the last glacial period affects dust volume-related measurements

Aaron Chesler[1,2,3], Dominic Winski[1,2], Karl Kreutz[1,2], Bess Koffman[4], Erich Osterberg[5], David Ferris[5], Zeta Thundercloud[5], Joseph Mohan[16], Jihong Cole-Dai[7], Mark Wells[8], Michael Handley[1], Aaron Putnam[2], Katherine Anderson[5], and Natalie Harmon[2]

[1]Climate Change Institute, University of Maine, Orono, Maine, 04469, USA
[2] School of Earth and Climate Sciences, University of Maine, Orono, Maine, 04469, USA
[3]Environmental Studies Program, Goucher College, Towson, Maryland, 04903, USA
[4]Department of Geology, Colby College, Waterville, Maine, 04903, USA
[5]Department of Earth Science, Dartmouth College, Hanover, New Hampshire, 03755, USA
[6]Ecology and Environmental Sciences, University of Maine, Orono, Maine, 04469, USA
[7]Department of Chemistry and Biochemistry, South Dakota State University, Brookings, South Dakota, 57007
[8]School of Marine Sciences, University of Maine, Orono, Maine, 04469, USA

Correspondence to: Aaron Chesler (aaron.chesler@maine.edu)

1.Contents of this file

1. Introduction

Table S1

Figures S1 to S12

2. Table S1

Table S1. Coincidence analysis results for r, r^2, and p-value for each run during the two time periods with the highest Abakus offset from the CC (Figure 2).

	Coincidence Test	R	R^2	p-value
Heinrich Stadial 1 (16-18ka)	5.1-6.4µm: <5.1 µm	-4.63×10^{-3}	2.14×10^{-5}	0.84
	3.2-6.4 µm: <3.2 µm	3.28×10^{-2}	1.08×10^{-3}	0.15
LGM (18-27ka)	5.1-6.4µm: <5.1 µm	-5.18×10^{-3}	2.69×10^{-5}	0.63
	3.2-6.4 µm: <3.2 µm	3.15×10^{-2}	9.91×10^{-4}	<0.01

2. Figures S1 to S10

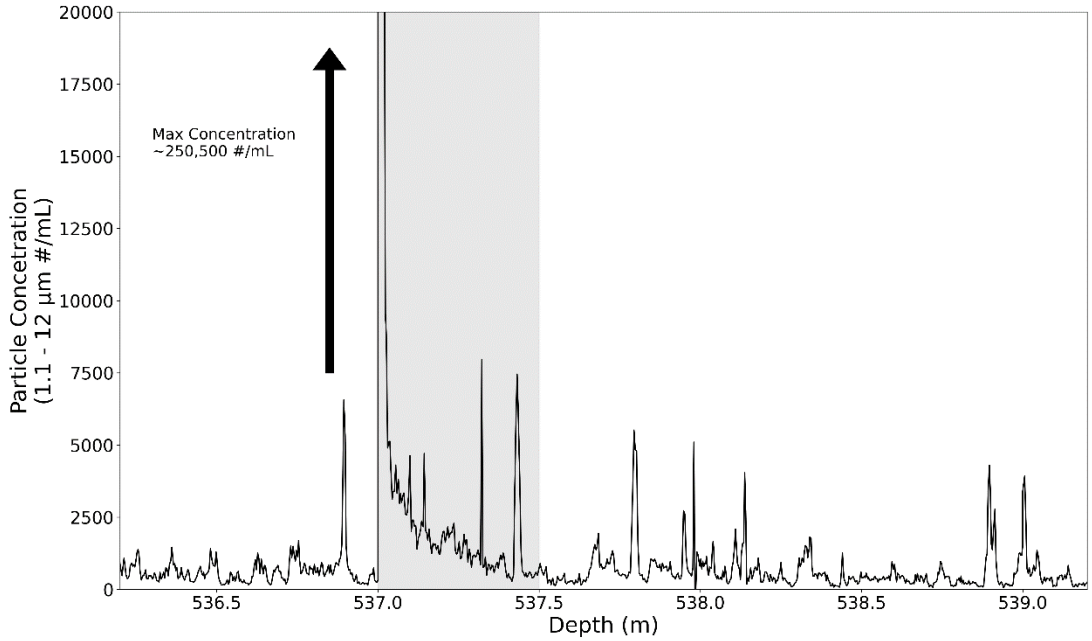

Figure S1. Estisol-140 style particle contamination highlighted in grey. Peak concentration is about 250,500 particles/mL Peak particle concentration is followed by a log scale decrease down core back to background concentration for the figure 523 ± 452 (536.2 – 539.2; standard error of the mean).

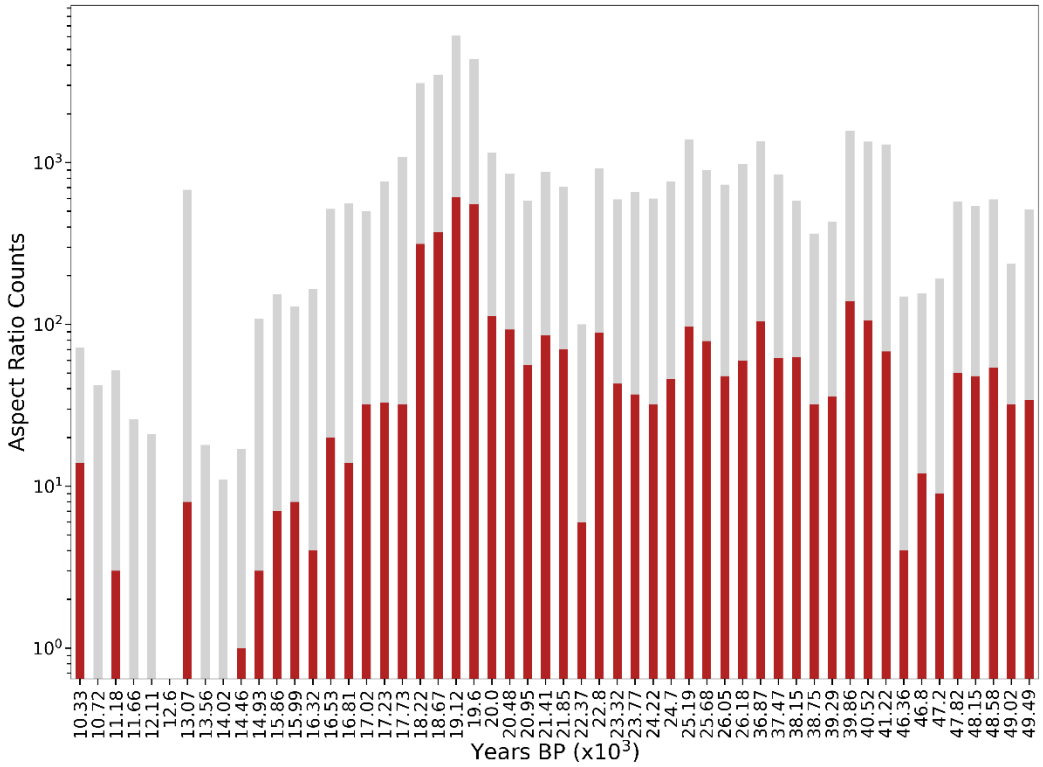

Figure S2. Particle counts per sample measured via DPI FlowCAM. Between 15 – 10 ka, there were low and inconsistent coarse particle counts in the DPI samples. Red colors are coarse (5.1 – 6.4 µm) particle counts and grey bars are total particle counts.

Figure S3. Subset of particle images captured from ~17.2 ka using FlowCAM.

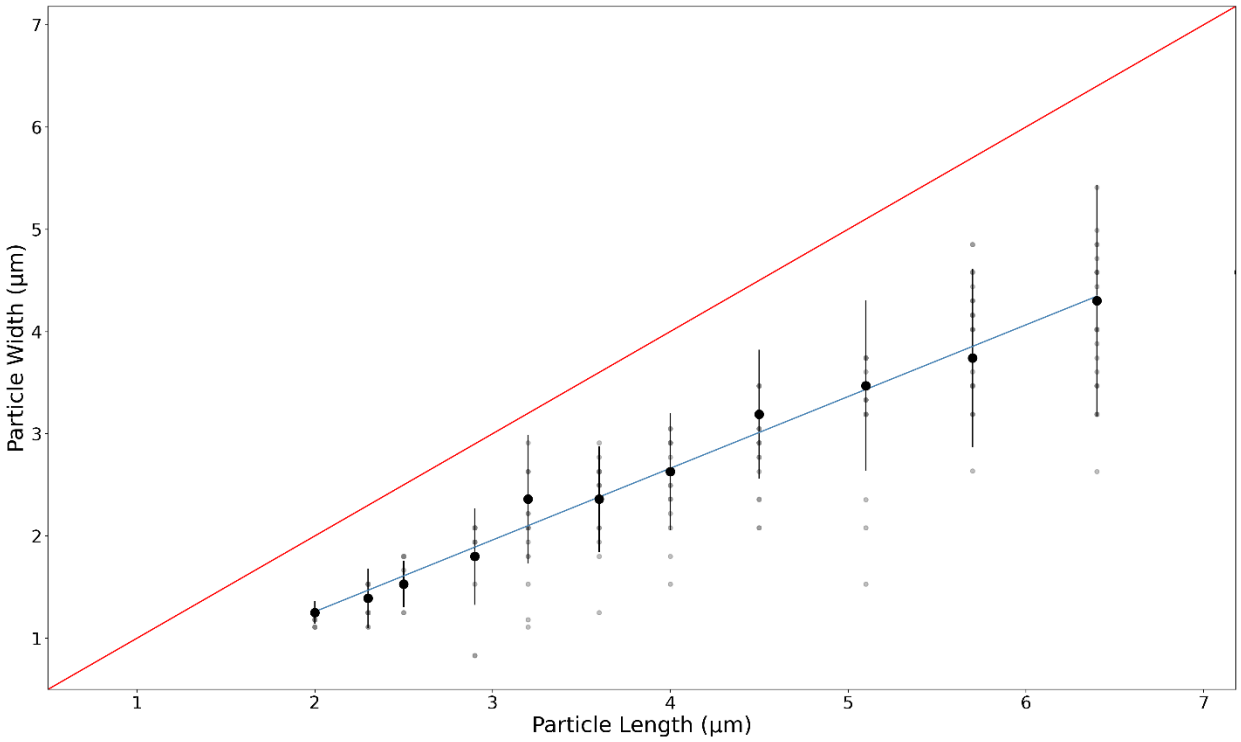

Figure S4: Averaged particle width measurements (µm; 2σ) by particle size information. Width measurements are not equal to length measurements (1:1 red line). The slope of the lines of best fit (blue) is 0.70, highlighting the incorrect assumption of non-equal particle dimensions.

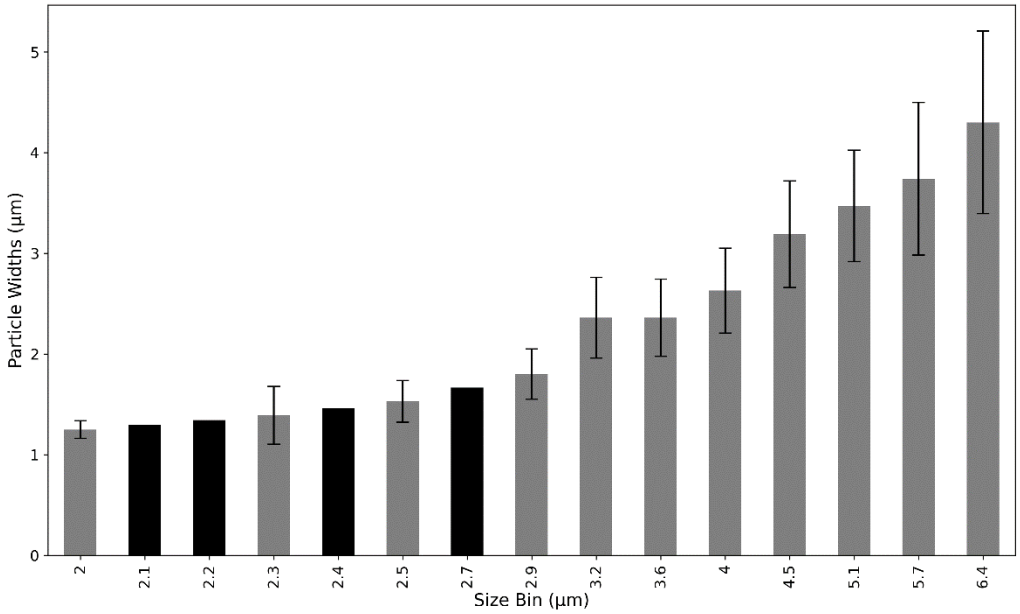

Figure S5: Differences in particle width measurements by Abakus bin size. Measurements in black have been derived from linear interpolation. Error bars represent the variability of average width measurements throughout the record by particle size. Particle width measurements between neighboring bins are within the 2 σ standard deviation of each other. Therefore, we calculate missing bin sizes using linear interpolation.

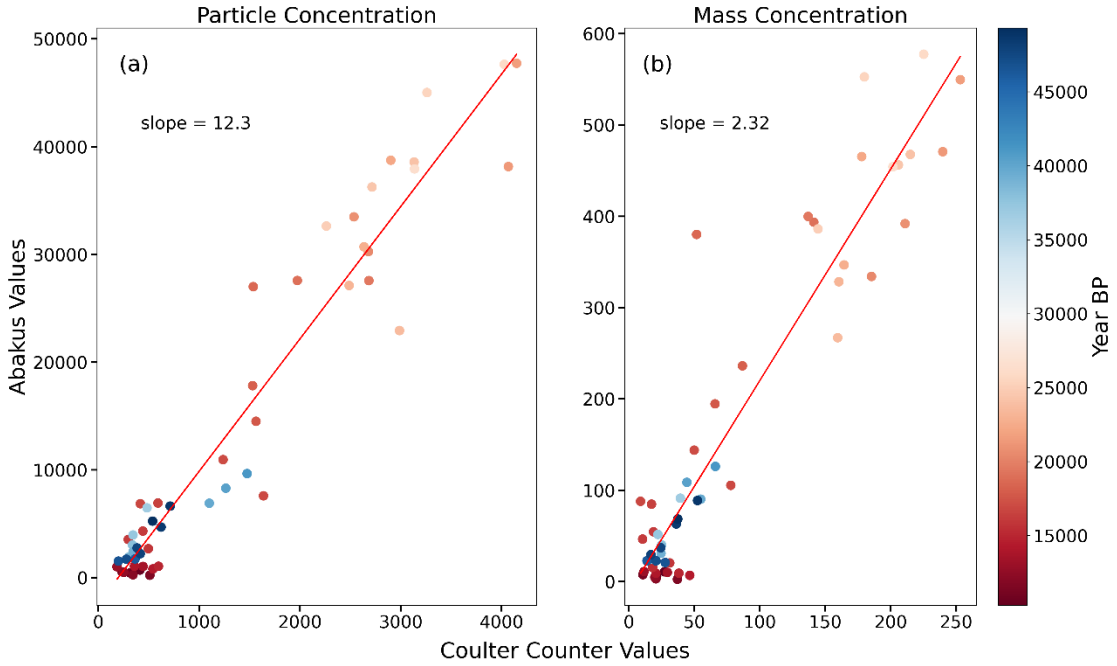

Figure S6. Scatterplots showing Abakus and Coulter Counter particle data from 54 periods analyzed: S4a) number concentration (r-value = 0.96, p-value < 0.01) and S4b) mass concentrations (r-value = 0.95, p-value < 0.01). Mass concentration was calculated using the assumption of spherical shape.

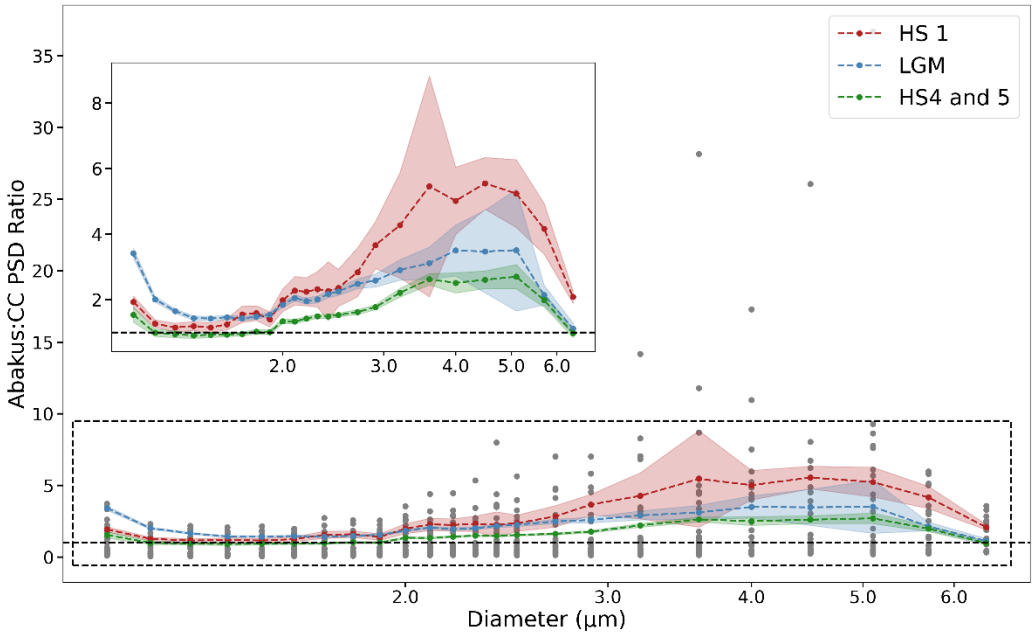

60

Figure S7. Particle size distribution ratios from the Abakus and Coulter Counter samples during HS 1 (18 – 16 ka; red), LGM (27 – 18 ka; blue), and HS 4 and 5 (42 – 36 ka; 50 – 46 ka; green). Colored regions represent one standard error of the mean for each time period. Inset is outlined by dashed box and highlights averaged ratio variability across bin sizes.

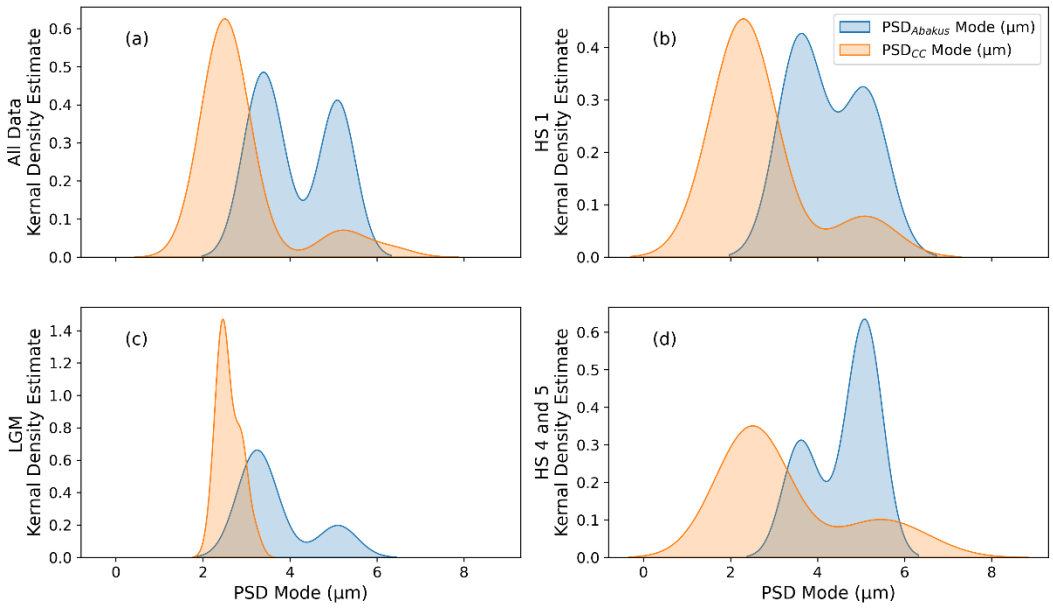

Figure S8: Mode distributions between the Abakus (blue) and CC (orange; 4a) All Data n = 41, 4b) HS1 n = 6; 4c) LGM n = 19; 4d) HS4 and 5 n = 16). PSD_{Abakus} and PSD_{CC} mode values were calculated for every comparative sample (i.e., averaged Abakus data and CC samples). Data are plotted using a kernel density estimate. Kernel density estimates are calculated from a probability density function as an estimate for continuous random variables.

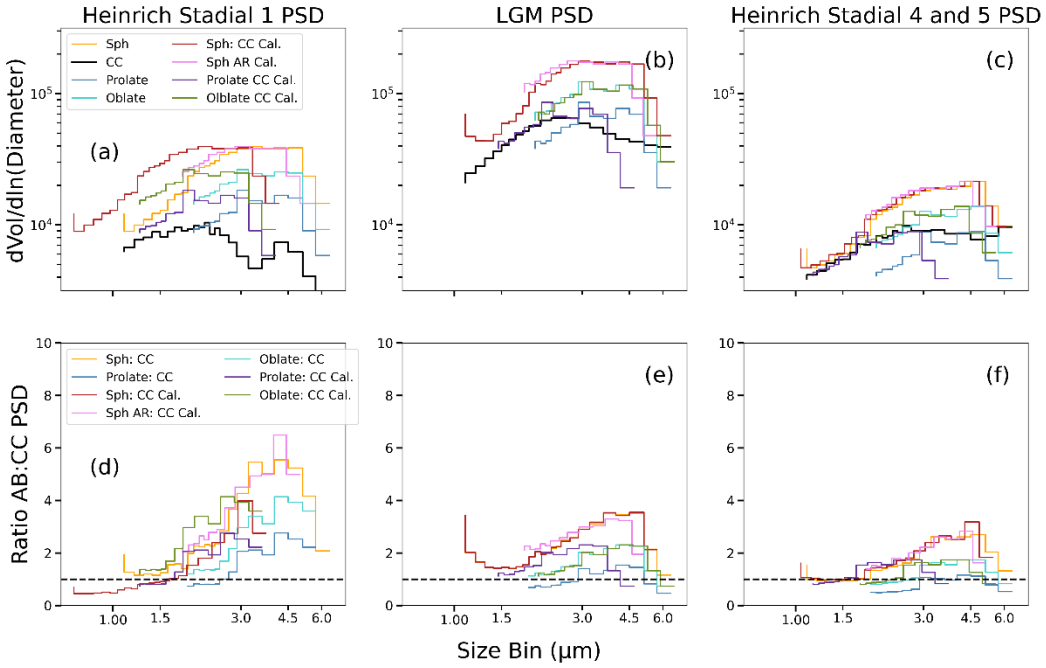

Figure S9: Comparison of Abakus volume and calibration schemes (Equations 1-3) and PSD_{CC}. Sph = AB sphere calculation, CC = CC calculation, El 1 = Ellipsoid 1 PSD calculation, El 2 = Ellipsoid 2 PSD calculation, Sph: CC Cal. = AB Spherical: CC calibration, Sph AR Cal. = Aspect Ratio calibration, El 1: CC Cal = Ellipsoid 1: CC calibration, El 2: CC Cal = Ellipsoid 2: CC calibration. The top panel (9a – c) compares the PSD_{Abakus} volume and calibration techniques to PSD_{CC} and the bottom panel (9d – f) is the ratio of each PSD_{Abakus} to the PSD_{CC} in different time periods. The dotted line represents a 1:1 value. There are clear temporal differences between each method used. Ellipsoid 1 and Ellipsoid 2 reduce the offset between spherical calculation and CC during the LGM and Heinrich Stadial 4 and 5.

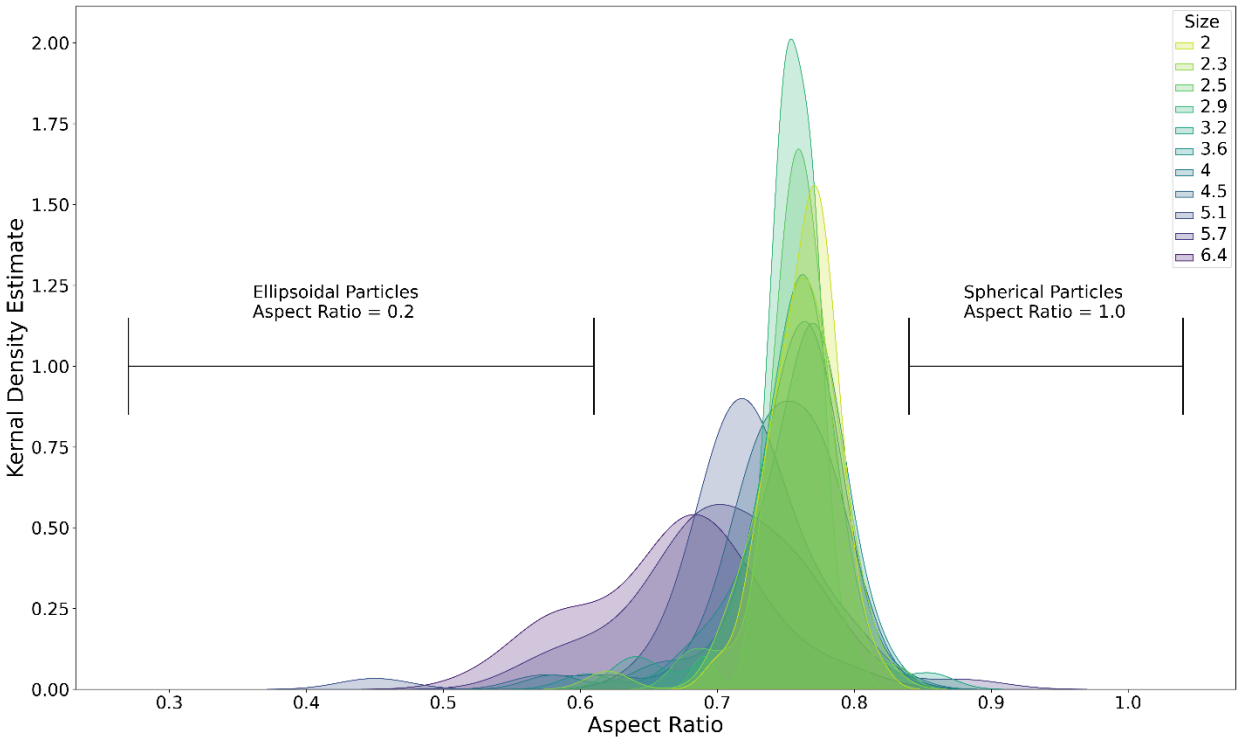

Figure S10. Abakus bin size-averaged and interpolated aspect ratio measurements determined using a FlowCAM. Error bars for Spherical and Ellipsoidal data were taken from Mathaes et al. (2020) for FlowCAM measurements under a 10x zoom. The error bars for two different aspect ratio measurements of 5 µm particles are shown for reference (Mathaes et al., 2020). It is likely that these error estimates are overly conservative as applied to our study because we used at 20x zoom factor (recommended by the FlowCam manual), whereas Mathaes et al. (2020) used a 10x zoom.

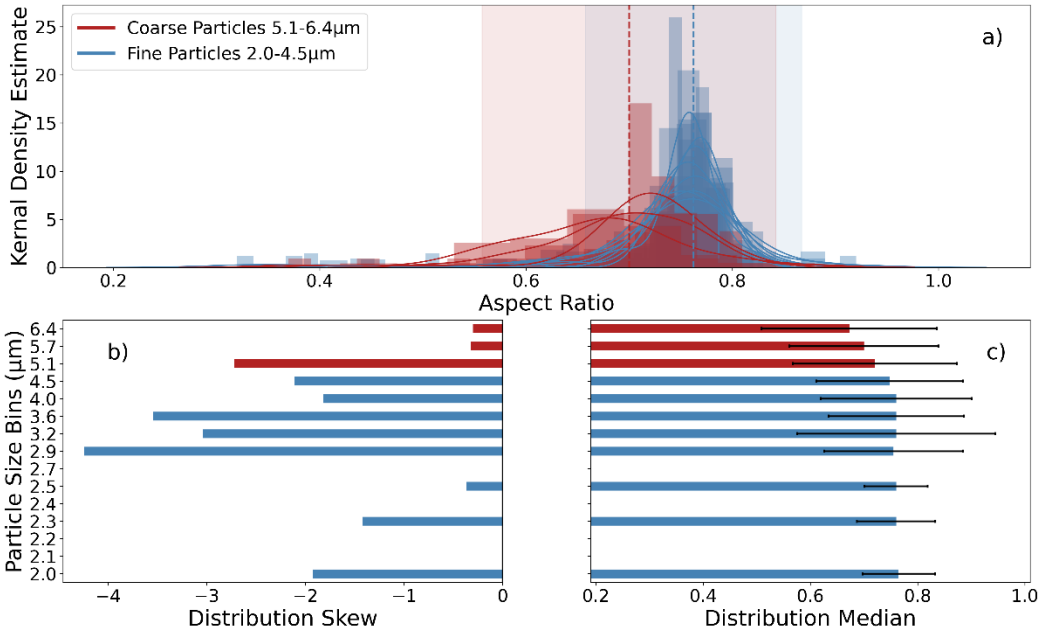

Figure S11a - c. S11a) Fine and coarse particle aspect ratio distributions with distribution skew and size bin median value with 2σ S.D. Regardless of particle size-bin, particle distribution statistics are leptokurtic and are skewed towards more elongated particles. Dotted lines and shading represent respective median values and standard deviation (2σ).

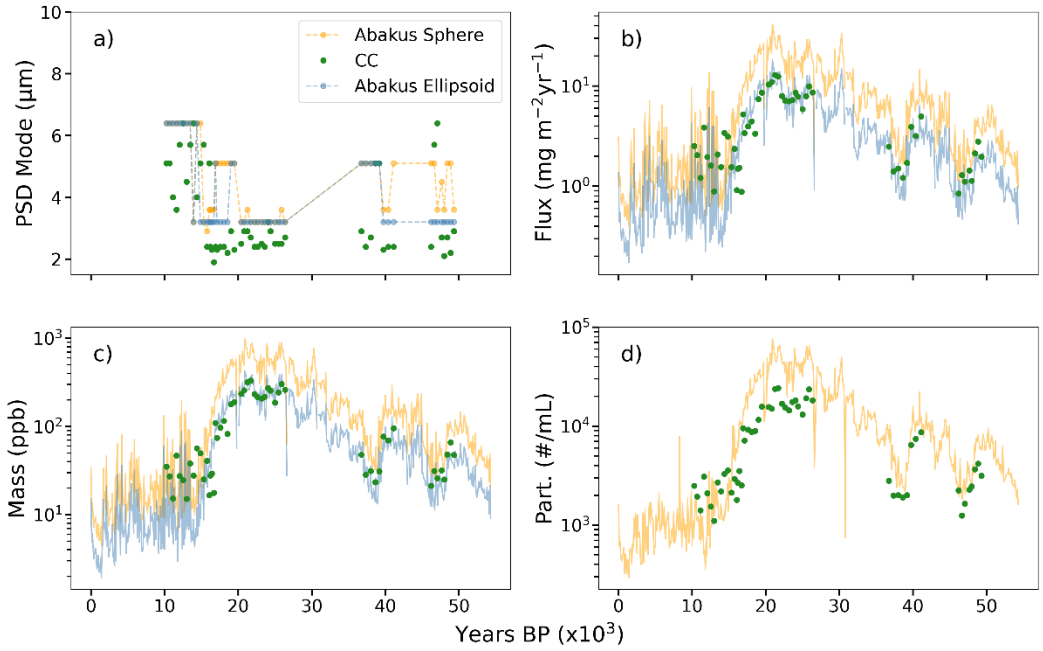

Figure S12a – d: 100-year resampled mean (12a – d) particle metrics. The resampled median values (Figure 5a – d) spanning 16 – 10 ka show discrepancy between the CC and Abakus samples, which the resampled mean values (12a – d) show a close correspondence between the two methodologies. We interpret the increased variability in the resampled mean values as an effect of Estisol-140. Because the natural concentration increases prior to 16 ka (i.e., during the LGM), we believe that any Estisol-140 contamination is mitigated by the naturally high dust concentration.

References

Mathaes, R., Manning, M. C., Winter, G., Engert, J., and Wilson, G. A., 2020, Shape Characterization of Subvisible Particles Using Dynamic Imaging Analysis: J Pharm Sci, v. 109, no. 1, p. 375-379.

Mathaes, R., Manning, M. C., Winter, G., Engert, J., and Wilson, G. A., 2020, Shape Characterization of Subvisible Particles Using Dynamic Imaging Analysis: J Pharm Sci, v. 109, no. 1, p. 375-379.

Mathaes, R., Manning, M. C., Winter, G., Engert, J., and Wilson, G. A., 2020, Shape Characterization of Subvisible Particles Using Dynamic Imaging Analysis: J Pharm Sci, v. 109, no. 1, p. 375-379.